Quantum Computing by Coherent Cooling

Jia-Jin Feng (冯嘉进) [ORCID],[1] Biao Wu (吴飙) [ORCID],[1,2,3,*] and Frank Wilczek[4,5,2,6,7]

[1]*International Center for Quantum Materials, School of Physics, Peking University, Beijing 100871, China*
[2]*Wilczek Quantum Center, School of Physics and Astronomy, Shanghai Jiao Tong University, Shanghai 200240, China*
[3]*Collaborative Innovation Center of Quantum Matter, Beijing 100871, China*
[4]*Center for Theoretical Physics, Massachusetts Institute of Technology, Cambridge, Massachusetts 02139, USA*
[5]*T. D. Lee Institute, Shanghai Jiao Tong University, Shanghai 200240, China*
[6]*Department of Physics, Stockholm University, Stockholm SE-106 91, Sweden*
[7]*Department of Physics, Arizona State University, Tempe, Arizona 25287, USA*

Interesting problems in quantum computation take the form of finding low-energy states of (pseudo)spin systems with engineered Hamiltonians that encode the problem data. Motivated by the practical possibility of producing very low-temperature spin systems, we propose and exemplify the possibility to compute by coupling the computational spins to a quantum coherent bath that serves as a heat sink. The quantum tunneling effect provides additional cooling channels to accelerate the cooling process. We demonstrate both analytically and numerically that this strategy can achieve a quantum advantage in the unstructured search problem.

I. INTRODUCTION

Quantum computing can be implemented, conceptually, using either quantum logic gates [1–4] or Hamiltonians [5,6]. Under broad assumptions, these two techniques are computationally equivalent, abstractly [7,8], but each brings in different methods and intuitions. Roughly speaking, the gate approach is more familiar in the analysis of Turing machines and practical digital circuits, while a Hamiltonian approach is more familiar in the analysis of natural physical systems. The quantum adiabatic approach to optimization problems [6,9,10] is an outstanding example suggested by a physical phenomenon, i.e., the preservation of quantum ground states under adiabatic evolution; other examples include algorithms inspired by resonance [11] and diffusion [12]. Physics can also suggest possibilities for resources that are not usually considered in the standard conceptual models, e.g., global addressing of qubits by external fields or controlled coupling to physically realistic heat sinks, as exemplified below.

The observation that many important computational problems can be encoded as the search for low-energy states of explicit, deceptively simple Hamiltonians H_s is central to applications of the adiabatic algorithm. One way to bring a system to low energy, of course, is to couple it to an auxiliary low-temperature system. The production of (pseudo)spin systems with very low temperature is a highly developed art [13–17]. Putting those observations together, we are led to consider the possibility of addressing computational problems by coupling systems whose ground states contain the answer—"computational qubits"—to systems that have very low temperatures—"bath qubits"—that act as an energy sink.

*wubiao@pku.edu.cn

The issue then arises whether this procedure can be performed in a way that maintains a speed advantage of quantum over classical computation. Here we demonstrate that it can, at least in the context of the iconic Grover search problem [1,18–20].

II. COOLING WITH A QUANTUM BATH

A. General framework

Let us first describe the strategy of our approach. Our computing scheme involves computational qubits and bath qubits. The problem Hamiltonian H_s encodes the solutions of a given problem in its ground states [21]. The bath Hamiltonian H_b is usually an interacting spin system with trivial ground states, so that it can be brought close to absolute zero temperature readily. For example, one may choose

$$H_b = -J \sum_{\langle m,m' \rangle} \left(\hat{\sigma}_m^x \hat{\sigma}_{m'}^x + \hat{\sigma}_m^y \hat{\sigma}_{m'}^y + \hat{\sigma}_m^z \hat{\sigma}_{m'}^z \right), \quad (1)$$

where $J > 0$ is the interaction strength and $\hat{\sigma}_m^{x,y,z}$ is the Pauli matrix of the mth spin. The summation is over an arbitrary set of qubit pairs $\langle m, m' \rangle$. This Hamiltonian has at least two trivial ground states $|00\cdots0\rangle$ and $|11\cdots1\rangle$ ($|0\rangle$ for spin-down and $|1\rangle$ for spin-up), which are easy to prepare. When the spins sit on a one-dimensional chain with the nearest-neighbor interaction, it is the well-known Heisenberg XXX model [22–24], and its spin-wave excitation can carry energy away from the problem system [25–27]. There are many interacting spin systems with trivial ground states [28].

We call our approach the quantum icebox algorithm, and its total Hamiltonian is

$$H = H_s + H_b + H_I, \quad (2)$$

where H_I is the coupling between computational qubits and bath qubits. $\langle H_I \rangle$ has the same order of magnitude as $\langle H_s \rangle$, which low order perturbation theory usually fails. There are n_s computational qubits and n_b bath qubits, so the Hilbert space size is $N_s = 2^{n_s}$ for H_s and $N_b = 2^{n_b}$ for H_b. Their energy eigenequations are $H_s |\psi_{i_s}\rangle = E_{i_s} |\psi_{i_s}\rangle$ and $H_b |\phi_{j_b}\rangle = E_{j_b} |\phi_{j_b}\rangle$, respectively. The total Hilbert space of size $N_c = N_s N_b$ is spanned by the base $|\psi_{i_s}\rangle \otimes |\phi_{j_b}\rangle \equiv |\psi_{i_s}, \phi_{j_b}\rangle$. Among all $|\psi_{i_s}\rangle$'s and $|\phi_{j_b}\rangle$'s, for clarity, we use $|\phi_{g_s}\rangle$ to denote the unknown ground states of the problem system H_s, which are the solutions of the problem, and $|\phi_{g_b}\rangle$ to denote the known ground state of the bath H_b, which is easy to prepare. The whole composite system is considered as a closed system in this icebox algorithm, which is distinct from other open systems with information loss in the bath. We set $\hbar = 1$ and consider E and t as dimensionless variables in the following discussion because they are irrelevant to time complexity, which is our focus.

We intend to use the bath to cool down the problem system and find its ground states $|\phi_{g_s}\rangle$. The bath is initialized in one of its trivial ground states $|\phi_{g_b}\rangle$, so that it is at the absolute zero temperature. The problem system can be initialized in an arbitrary state that is easy to prepare. So, the full initial wave function at $t = 0$ is

$$|\Psi_{in}\rangle = \sum_{i_s=0}^{N_s-1} c_{i_s} |\psi_{i_s}, \phi_{g_b}\rangle, \quad (3)$$

where c_{i_s} is the superposition probability amplitude. Once the interaction H_I is turned on, the whole composite system starts the evolution with $|\Psi\rangle = e^{-iHt} |\Psi_{in}\rangle$ and the energy will generally flow from the problem system to the bath. As a result, the problem system is cooled and will get closer to its ground state. If we measure the problem system at the end of cooling, we will have the following probability for finding the ground state $|\phi_{g_s}\rangle$ of the problem system H_s:

$$P_g = \sum_{j_b=0}^{N_b-1} |\langle \phi_{g_s}, \phi_{j_b} | \Psi \rangle|^2. \quad (4)$$

The aim of the icebox cooling algorithm is to make this probability high in the shortest amount of time.

B. Toy model

To get oriented, let us briefly consider a toy example. The system is a single spin coupled to the middle spin of a one-dimensional spin chain,

$$H_s = B\hat{s}^z, \quad H_i = \lambda \hat{s}^y \hat{\sigma}^y_{\lfloor \frac{n_b}{2} \rfloor}, \quad (5)$$

where B is the on-site energy, λ is the coupling strength, and $\lfloor n_b/2 \rfloor$ means that the biggest integer is smaller than or equal to $n_b/2$. The bath is a one-dimensional spin chain governed by the Hamiltonian in Eq. (1) with the nearest-neighbor interaction and periodic boundary condition.

The system spin is set in the excited state and the bath is set in the ground state with all spins down. After the interaction is turned on instantaneously, the energy begins to flow into the bath, generating spin-wave excitations that carry away energy from the problem system [29,30]. Numerical results
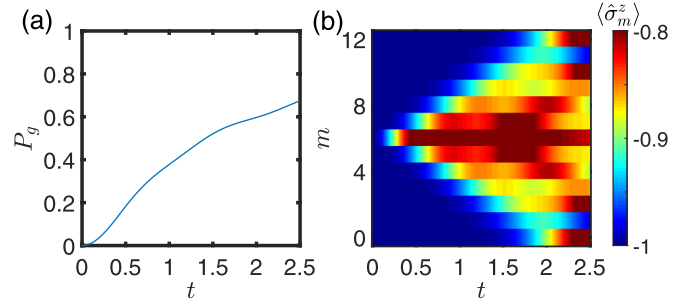

FIG. 1. (a) The ground-state probability of the system in Eq. (5). (b) The color is the z direction component of each qubit in the bath. m marks different qubits. Other parameters are $n_s = 1$, $n_b = 13$, $J = 1$, $B = 1$, $\lambda = 1$, and $|\Psi_{in}\rangle = |e_s, g_b\rangle$.

are shown in Fig. 1. In Fig. 1(a), the probability of the system in the ground state becomes larger with time. Meanwhile, the energy spreads away from the middle of the chain as shown in Fig. 1(b) (see Appendix A for an analytical approach).

III. UNSTRUCTURED SEARCH

Now we apply that general strategy to an unstructured search. An unstructured search is a benchmark example demonstrating a sharp difference between quantum and classical computers. To search M targets among N unsorted items, the time complexity of a classical algorithm is $O(N/M)$. In contrast, Grover's algorithm on a quantum computer has a time complexity of $O(\sqrt{N/M})$ [31,32]. When our cooling algorithm is applied to this search problem, we expect a time complexity no better than $O(\sqrt{N_c/N_b} = \sqrt{N_s})$. The reason is that all the N_b states $|\psi_{g_s}, \phi_{j_b}\rangle$'s are the targets among the total $N_c = N_s N_b$ states $|\psi_{i_s}, \phi_{j_b}\rangle$ for the whole system.

In our quantum algorithm, all the search items are stored in system qubits and encoded by states $|i_s\rangle$ where the mth system qubit is in the state $|i_s^{(m)}\rangle$ ($m = 0, 1, 2, \ldots, n_s - 1$), with $i_s^{(m)}$ being the binary digit of i_s. For simplicity, we consider the case in which there is only one target, which is one of the $|i_s\rangle$. We construct two Hamiltonians, respectively, for the problem system and the bath as [5,9,11,33,34]

$$H_s = -|g_s\rangle \langle g_s|, \quad H_b = -|g_b\rangle \langle g_b|. \quad (6)$$

These two Hamiltonians have only two eigenenergies, respectively, one for a nondegenerate ground state and the other for highly degenerate excited states (see Fig. 2). The system ground state $|g_s\rangle$ encoding the target is unknown while the
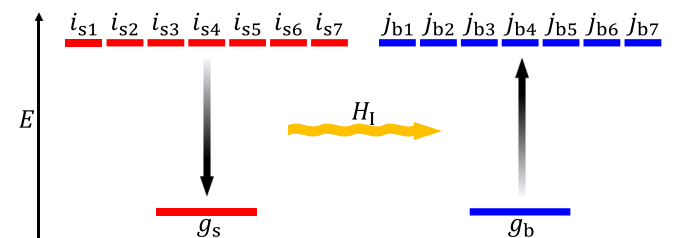

FIG. 2. The diagram of the Hamiltonian $H = H_s + H_b + H_I$ for unstructured search. The red bars are the energy levels of H_s. The blue bars are the energy levels of H_b.

bath ground state $|g_{\rm b}\rangle$ is known and can be assumed to be $|g_{\rm b}\rangle = |000\cdots 0\rangle$ without loss of generality. For the above two Hamiltonians, their energy eigenstates are simply $|\psi_{i_{\rm s}}\rangle = |i_{\rm s}\rangle$ and $|\phi_{j_{\rm b}}\rangle = |j_{\rm b}\rangle$, respectively. Our quantum algorithm works to find the system's ground state $|g_{\rm s}\rangle$ by coupling the system to the bath.

To achieve a quantum advantage, one must be able to flip the order of $O(n_{\rm s})$ qubits for the problem system coherently together. This can be realized clearly with a nonlocal interaction. It can also be accomplished with coherently iterated k-local interactions. We will show that both of them can outperform the classical algorithm.

A. Nonlocal interaction

Here we choose the following nonlocal interaction to couple the system to the bath:

$$H_{\rm I} = -|\xi\rangle\langle\xi|,\qquad(7)$$

where $|\xi\rangle = \sqrt{1/N_{\rm c}}\sum_{i_{\rm s}=0}^{N_{\rm s}-1}\sum_{j_{\rm b}=0}^{N_{\rm b}-1}|i_{\rm s},j_{\rm b}\rangle$. Similar nonlocal interactions can be found in Refs. [5,9,11,33,34] and their justification can be found in Appendix B.

The initial state for the whole system is

$$|\Psi_{\rm in}\rangle = \frac{1}{\sqrt{N_{\rm s}}}\sum_{i_{\rm s}=0}^{N_{\rm s}-1}|i_{\rm s},g_{\rm b}\rangle,\qquad(8)$$

where the bath is in the ground state. The dynamics is confined in a subspace spanned by the following four states: $|y_{\rm s},y_{\rm b}\rangle$, $|g_{\rm s},y_{\rm b}\rangle$, $|y_{\rm s},g_{\rm b}\rangle$, and $|g_{\rm s},g_{\rm b}\rangle$ with $|y_{\rm s}\rangle = \sqrt{1/(N_{\rm s}-1)}\sum_{i_{\rm s}\neq g_{\rm s}}|i_{\rm s}\rangle$ and $|y_{\rm b}\rangle = \sqrt{1/(N_{\rm b}-1)}\sum_{j_{\rm b}\neq g_{\rm b}}|j_{\rm b}\rangle$. In other words, the Hamiltonian is effectively a 4×4 matrix shown in Appendix C. In the limit of $1\ll N_{\rm s},N_{\rm b}\ll N_{\rm c}$, this matrix can be diagonalized exactly. As $|\Psi_{\rm in}\rangle = \sqrt{1/N_{\rm s}}|g_{\rm s},g_{\rm b}\rangle + \sqrt{(N_{\rm s}-1)/N_{\rm s}}|y_{\rm s},g_{\rm b}\rangle$, its time evolution is

$$
\begin{aligned}
|\Psi\rangle \approx\ & e^{-2it}\sqrt{\frac{1}{N_{\rm s}}}|g_{\rm s},g_{\rm b}\rangle\\
& + e^{-it}\sqrt{\frac{N_{\rm s}-1}{N_{\rm s}}}\bigg[\frac{N_{\rm s}\cos\omega t + N_{\rm b}}{N_{\rm s}+N_{\rm b}}|y_{\rm s},g_{\rm b}\rangle\\
& + \frac{\sqrt{N_{\rm s}N_{\rm b}}(\cos\omega t - 1)}{N_{\rm s}+N_{\rm b}}|g_{\rm s},y_{\rm b}\rangle\\
& + i\sqrt{\frac{N_{\rm s}}{N_{\rm s}+N_{\rm b}}}\sin\omega t\,|y_{\rm s},y_{\rm b}\rangle\bigg],
\end{aligned}\qquad(9)
$$

where the oscillation frequency is

$$\omega \approx \sqrt{\frac{1}{N_{\rm s}}+\frac{1}{N_{\rm b}}}.\qquad(10)$$

We can substitute Eq. (9) into Eq. (4) and obtain

$$P_g \approx \frac{4N_{\rm s}N_{\rm b}}{(N_{\rm s}+N_{\rm b})^2}\sin^4\frac{\omega t}{2}.\qquad(11)$$

For the special case $N_{\rm b} = N_{\rm s}$, we have $P_g \approx 1$ at $t = \pi\sqrt{N_{\rm s}/2}$. The time complexity of our algorithm is $O(\sqrt{N_{\rm s}})$, which is as good as Grover's algorithm [1]. In general, the average time

needed to finish this algorithm is

$$\overline{T} = \frac{\pi}{\max(P_g)_t\,\omega} = \frac{\pi(N_{\rm s}+N_{\rm b})^{1.5}}{4\sqrt{N_{\rm s}N_{\rm b}}}.\qquad(12)$$

When $N_{\rm b} = 0.5N_{\rm s}$, the required time is shortest with $\overline{T} = 2.04\sqrt{N_{\rm s}}$. When $N_{\rm b}\ll N_{\rm s}$, the time complexity is $O(N_{\rm s})$, which is similar to the classical algorithm. The reason is that there are not enough high-energy states in a small bath to absorb energy. When $N_{\rm b}\gg N_{\rm s}$, the time complexity is $O(N_{\rm b}/\sqrt{N_{\rm s}})$ because the effective interaction becomes small.

B. Local interaction

Our cooling algorithm can also achieve speedup over the classical algorithm with local interactions. We focus on the case $n_{\rm b} = n_{\rm s}$. The two-local interaction is

$$H_{\rm I} = -\lambda_{n_{\rm s}}\sum_{m=0}^{n_{\rm s}-1}\hat{s}_m^x\hat{\sigma}_m^x,\qquad(13)$$

where $\hat{s}_m^x$ and $\hat{\sigma}_m^x$ acts on the mth qubit of the problem system and the bath, respectively. $\lambda_{n_{\rm s}}$ is the interaction strength. $\lim_{n_{\rm s}\to\infty}\lambda_{n_{\rm s}}\times n_{\rm s}$ is a constant that makes $\langle H_{\rm I}\rangle$ and $\langle H_{\rm s}\rangle$ the same order of magnitude. This composite system can be viewed as two parallel spin chains with pairwise coupling (see Fig. 5).

The dynamics governed by H is a unitary evolution in a Hilbert space of dimension $N_{\rm c} = N_{\rm s}N_{\rm b} = N_{\rm s}^2$. Fortunately, it can be decomposed into $N_{\rm s}$ independent dynamics with each of them restricted in an $N_{\rm s}$-dimensional sub-Hilbert space. Each subspace $\mathscr{H}_\nu$, which is marked by a binary string ν, is spanned by states $|i_{\rm s}\rangle\otimes|j_{\rm b}\rangle$ that satisfy the bitwise logical operation $\nu = i_{\rm s}\oplus j_{\rm b}$ explained in Appendix D.

We still choose Eq. (8) as the initial state, where different $i_{\rm s}$'s belong to different subspaces $\mathscr{H}_{\nu_{i_{\rm s}}}$ labeled by $\nu_{i_{\rm s}} = i_{\rm s}\oplus g_{\rm b}$. In a given subspace $\mathscr{H}_{\nu_{j_{\rm s}}}$ ($j_{\rm s}$ is one of $i_{\rm s}$'s), we can hide the bath qubits and simplify the total Hamiltonian as (details for derivation can be found in Appendix E)

$$H_{j_{\rm s}} = -|g_{\rm s}\rangle\langle g_{\rm s}| - |j_{\rm s}\rangle\langle j_{\rm s}| - \lambda_{n_{\rm s}}\sum_{m=0}^{n_{\rm s}-1}\hat{s}_m^x.\qquad(14)$$

The system described by the above Hamiltonian is a double-well system in Fig. 3(a). It can be visualized as a particle living on a hypercube of $n_{\rm s}$ dimensions in Fig. 3(b). Each site of this hypercube is represented by a state $|i_{\rm s}\rangle$. Only two of these sites, $|g_{\rm s}\rangle$ and $|j_{\rm s}\rangle$, have lower on-site energy.

For this kind of system, the low-energy Hilbert space is spanned by two wave packets $|\chi_g\rangle$ and $|\chi_j\rangle$ localized near $|g_{\rm s}\rangle$ and $|j_{\rm s}\rangle$, respectively. This is verified by our numerical computation. In our numerical computation, we expand the interaction strength in the polynomial form

$$\lambda_{n_{\rm s}} = \frac{\gamma_1}{n_{\rm s}}+\frac{\gamma_2}{n_{\rm s}^2}+\frac{\gamma_3}{n_{\rm s}^3}+\cdots.\qquad(15)$$

We then diagonalize numerically the Hamiltonian of Eq. (14). As we expect that the two lowest eigenstates are of the form $(|\chi_g\rangle + |\chi_j\rangle)/\sqrt{2}$ and $(|\chi_g\rangle - |\chi_j\rangle)/\sqrt{2}$ if $j\neq g$, we superpose them and obtain $|\chi_g\rangle$. As shown in Fig. 3(c), we find that $|\chi_g\rangle$ is indeed localized and its localization will not decrease as $n_{\rm s}$ increases if $\gamma_1\lesssim 1$, $\gamma_2\lesssim 1.16$, and $\gamma_{m\geqslant 3} = 0$.
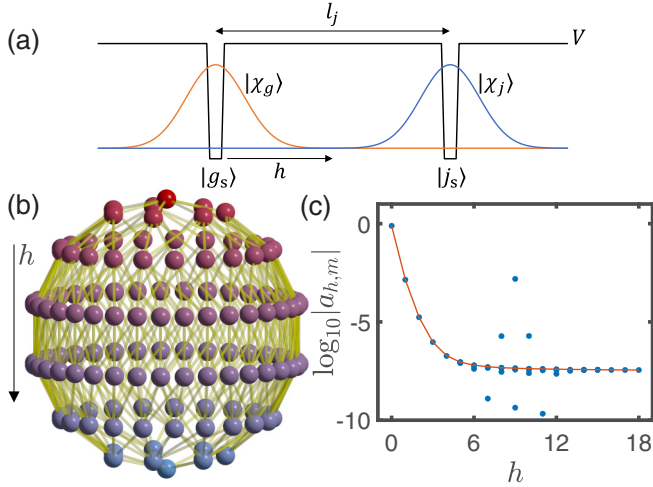
FIG. 3. (a) One-dimensional schematic illustration of Hamiltonian H_{j_s}. $|\chi_g\rangle$ and $|\chi_j\rangle$ are the low-energy wave packets in the wells. (b) Schematic of the n_s-dimensional hypercube (placed on a hypersphere). Each point represents one configuration of qubits with the top point representing $|g_s\rangle$. The color represents the Hamming distance h of $|i_s\rangle$ from $|g_s\rangle$ (red for smaller distance, blue for larger distance). Yellow lines represent hopping between different $|i_s\rangle$. (c) The actual wave function of one wave packet $|\chi_g\rangle$ (blue dots) reconstructed by diagonalizing Eq. (14). $|j_s\rangle$ locates at $l_j = 9$ for example. The number of qubits is $n_s = 18$. The interaction strength is $\gamma_1 = 1$, $\gamma_2 = 1.16$, and $\gamma_{m\geqslant 3} = 0$. The calculated well component is $|a_0|^2 = 0.8$. The orange line is the median among the same h.

The two wave packets $|\chi_g\rangle$ and $|\chi_j\rangle$ have the same on-site energy. Their interaction strength decides the oscillation frequency $\omega_{l_j} = |\langle\chi_g| H |\chi_j\rangle|$, which is the evolution speed from $|j_s\rangle$ to $|g_s\rangle$. The Hamming distance between two binary strings is the number of bits where they differ. We define the Hamming distance between $|g_s\rangle$ and $|j_s\rangle$ as l_j, which ranges from 0 to n_s. The dynamics in the subspaces with identical Hamming distance l_j is exactly the same. As the effective interaction decays with Hamming distance, i.e., $\omega_{l_j+1} < \omega_{l_j}$, the evolution time from $|j_s\rangle$ to $|g_s\rangle$ is longer for larger l_j.

When the problem system evolves into $|g_s\rangle$ through tunneling from the initial state of Eq. (8), it is cooled down by the bath and our goal is achieved. It is clear that the larger the Hamming distance l_j, the longer it takes to get $|g_s\rangle$. The longest time occurs when $l_j = n_s$. However, to have a detectable ground-state probability, we just need to wait until half of the states with $l_j \leqslant \lfloor n_s/2 \rfloor$ evolve to $|g_s\rangle$. On average, the ground-state probability can thus be approximated as

$$\overline{P_g} \approx \frac{1}{N_s}\left(A_0 + \sum_{l=1}^{\lfloor\frac{n_s}{2}\rfloor} C_{n_s}^l \overline{A_l \sin^2 \omega_l t}\right) \approx \frac{\overline{A_l}}{4}, \qquad (16)$$

where t is in the timescale regime $1/\omega_{\lfloor n_s/2 \rfloor} < t < 1/\omega_{\lfloor n_s/2 \rfloor+1}$ and A_l is the oscillation amplitude of a scale around 1. It is clear that the ground-state probability is large enough for detection and independent of n_s.

The cooling speed is roughly decided by $\omega_{\lfloor n_s/2 \rfloor}$, which is the energy difference of two lowest energy states in the subspace. Figure 4 shows the dependence of the cooling
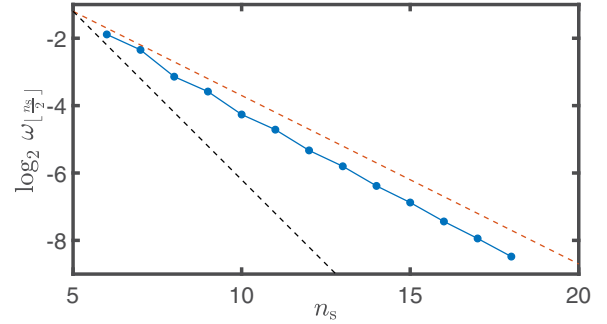

FIG. 4. The oscillation frequency between $|j_s\rangle$ and $|g_s\rangle$ with distance $l_j = \lfloor n_s/2 \rfloor$ according to Eq. (14). The blue dots are the exact value from diagonalization whose slope is about -0.55. The interaction strengths γ_m's are the same as Fig. 3. The slope of the orange dashed line is -0.5 representing Grover's algorithm. The slope of the black dashed line is -1 representing the classical algorithm.

speed on the number of qubits n_s. It is calculated by numerically diagonalizing Eq. (14) with $l_j = \lfloor n_s/2 \rfloor$. By fitting the numerical result, we find that the cooling speed is about $O(N_s^{0.55})$ with local interaction, which is close to Grover's algorithm [1].

C. Discussion and conclusion

We have presented two different cooling algorithms to do a random search. In the first algorithm, the coupling between the system and the bath is simple but nonlocal. The analytical solution shows that its time complexity is $O(\sqrt{N_s})$. In the second algorithm, the coupling is local. Our analysis and numerical computation find that the time complexity is $\sim O(N_s^{0.55})$. Both of the algorithms are parametrically faster than the classical time complexity $O(N_s)$. This is similar to the demonstration that the quantum adiabatic algorithm (QAA) is better than the conventional cooling [9,35] as argued in Appendix F. Thus our cooling algorithm incorporates essentially quantum features, and it differs from thermal cooling with a Markovian bath both qualitatively and quantitatively.

IV. GENERAL DISCUSSION

We have proposed a general framework of quantum computing by cooling a Hamiltonian system, whose ground states encode the solutions of a given problem, with a fully quantum bath in non-Markovian dynamics. This bath, which we call a quantum icebox, is an interacting (psuedo)spin system with trivial and easy-to-prepare ground states.

Here are the key features of our quantum icebox cooling scheme:

(i) It is different from cooling with a Markovian thermal bath. All the processes here are quantum coherent, enabling quantum tunneling over a long Hamming distance.

(ii) As the bath has easy-to-prepare ground states, it can be reset to zero temperature whenever necessary. We expect that resetting occasionally, by removing noisy feedback, will improve the success rate. This is a direction to be explored in the future.

(iii) A large density of states of the bath is favorable. The result is that efficient quantum transitions occur when the final state $|\psi_{i'_s}, \phi_{j'_b}\rangle$ has similar energy to the initial state $|\psi_{i_s}, \phi_{g_b}\rangle$, namely $E_{i'_s} + E_{j'_b} \approx E_{i_s} + E_{g_b}$. It is noteworthy that in the standard formulation of combinatorial optimization problems using penalty functions, the eigenenergies of H_s are integer multiples of a single parameter Δ. This consideration can guide the design of baths with appropriate energy spectra.

(iv) The number of states in the bath should increase rapidly with energy. This encourages the bath to absorb energy from the problem system. This is satisfied in most many-body systems, where higher energy can excite more quasiparticles. If the quasiparticles are weakly interacting, the growth is exponential.

(v) The total Hamiltonian need not change during execution of the quantum icebox algorithm. In contrast, QAA requires drawn-out and extensive change of the Hamiltonian during evolution, which requires external interventions introducing noise and decoherence.

Heat transfer has long been regarded as a stochastic thermal process [36–38], which is usually solved in a Markovian approximation, which is appropriate for infinitesimally weak interactions. In these Markovian models, only low-order transition is considered, while higher-order transitions involving tunneling effects discussed in Appendix G are absent [39–42] or not analyzed [43]. As a result, a quantum advantage cannot be achieved. It has been shown, within a one-dimensional solvable model, that cooling with the Markovian effect [44,45] has no speed advantage over the classical algorithm [46]. Stronger interaction can bring distinct dynamics [45], but they are difficult to assess generically. In Appendix H, we also compare our icebox algorithm with the quantum adiabatic algorithm (QAA) [35] and a fix-point quantum search [47], heat-bath algorithmic cooling (HBAC) [48–52], and interaction-enhanced quantum computing [53].

Our simulation of a quantum icebox demonstrates that cooling can occur coherently, and that it leads to a significant quantum computational advantage in a simple benchmark problem. (Other recent work also indicates that a non-Markovian bath could improve the performance of a quantum refrigerator [54].) In more complex optimization problems, the presence of low-lying local minima is generic. It is not implausible that weak coupling to a strongly ergodic bath will induce effective interactions that enable the coupled computational system to explore its state space thoroughly. This important question deserves much further attention, and it is the subject of ongoing research.

APPENDIX A: SPIN-WAVE PROPAGATION TRANSPORTING ENERGY

The spin-wave dynamics with the Hamiltonian Eq. (5) in the main text can also be demonstrated in the single excited mode approximation, where we consider just states $|e_s, k_g\rangle$ and $|g_s, k\rangle$, neglecting the states with multimagnon. $|g_s\rangle$ and $|e_s\rangle$ represent the ground state and the excited state of the problem system, while $|k_g\rangle$ and $|k\rangle$ represent the ground state and the excited state of the bath with wave vector k. The Hamiltonian becomes

$$H = \sum_{k \neq k_g} [\Delta E_k |g_s, k\rangle \langle g_s, k|$$
$$+ \lambda_k |g_s, k\rangle \langle e_s, k_g| + \lambda_k^* |e_s, k_g\rangle \langle g_s, k|], \quad \text{(A1)}$$

where $\Delta E_k = (E_{sg} + E_{bk}) - (E_{se} + E_{bk_g})$ is the energy detuning and λ_k is the coupling strength. The time-dependent wave function is

$$|\Psi\rangle = b_g |e_s, k_g\rangle + \sum_{k \neq k_g} b_k |g_s, k\rangle, \quad \text{(A2)}$$

where the probability amplitude satisfies the Schrödinger equation with

$$i\frac{db_g}{dt} = \sum_{k \neq k_g} \lambda_k^* b_k,$$

$$i\frac{db_k}{dt} = \Delta E_k b_k + \lambda_k b_g. \quad \text{(A3)}$$

In the early time of evolution $|\lambda_k| t \to 0$, $b_g \approx 1$. We can decouple the equations and get [55]

$$b_k \approx \frac{\lambda_k}{\Delta E_k}(e^{-i\Delta E_k t} - 1). \quad \text{(A4)}$$

The probability amplitude for the two-level system in its excited state is

$$b_g \approx 1 - 2 \sum_{k \neq k_g} \frac{|\lambda_k|^2}{\Delta E_k^2} \sin^2 \frac{\Delta E_k t}{2}. \quad \text{(A5)}$$

In the position coordinate, the wave function is

$$\phi \approx b_g e^{ik_g x} + \sum_{k \neq k_g} b_k e^{ikx}. \quad \text{(A6)}$$

The phase difference between different b_k changes with time, and the wave function will spread out from $x = 0$.

APPENDIX B: NONLOCALITY OF HAMILTONIANS

The Hamiltonians used in quantum algorithms should be physically plausible. This often means that the Hamiltonian should be k-local, i.e., the interactions involve no more than a fixed number k of qubits [7]. Although the three Hamiltonians in Eqs. (6) and (7) in the main text are not k-local, they are physically plausible, as we now explain.

In Grover's algorithm, a single Grover iteration is $U_G = R_\xi R_g$ [20]. $R_g = \mathbb{I} - 2|g\rangle\langle g|$ is the oracle operator for the target $|g\rangle$. The oracle operator is given as part of the statement in the problem. And $R_\xi = H_a^{\otimes n}(\mathbb{I} - 2|0\rangle\langle 0|)H_a^{\otimes n} = \mathbb{I} - 2|\xi\rangle\langle\xi|$, where H_a is the Hadamard gate and $|\xi\rangle = \sqrt{1/N} \sum_{j=0}^{N-1} |j\rangle$.

The Hamiltonians in Eqs. (6) and (7) in the main text can be implemented with the Grover operation U_G. For simplicity, we consider the Hamiltonian dynamics $U = e^{-iHt}$ with $H = -|g\rangle\langle g| - |\xi\rangle\langle\xi|$. When the time evolution is discretized with time step $\Delta t = \pi$ and $T = m\Delta t$, we have [56]

$$U = e^{-iHT} \approx \Pi_{j=1}^{m} e^{-i\pi H} \approx \Pi_{j=1}^{m} U_G. \tag{B1}$$

Note that the circuit complexity for implementing the oracle is $O(n^3)$ [57] and the time complexity is $O(n^2)$ [58], where $n = \log_2 N$.

Furthermore, this nonlocal interaction can be achieved by Mølmer-Sørensen (MS) interaction [34,59] or Rydberg atoms [60].

APPENDIX C: EXACT HAMILTONIAN FOR THE NONLOCAL MODEL

The total Hamiltonian is [Eqs. (6) and (7) in the main text]

$$H = -|g_s\rangle\langle g_s| - |g_b\rangle\langle g_b| - |\xi\rangle\langle\xi|. \tag{C1}$$

We expand it in terms of $|y_s, y_b\rangle$, $|g_s, y_b\rangle$, $|y_s, g_b\rangle$, and $|g_s, g_b\rangle$ with $|y_s\rangle = \sqrt{1/(N_s-1)}\sum_{i_s \neq g_s}|i_s\rangle$ and $|y_b\rangle = \sqrt{1/(N_b-1)}\sum_{j_b \neq g_b}|j_b\rangle$. Its exact matrix is

$$H = -\frac{1}{N_c}\begin{pmatrix} N_c - N_s - N_b + 1 & \sqrt{(N_c - N_s - N_b + 1)(N_b - 1)} & \sqrt{(N_c - N_s - N_b + 1)(N_s - 1)} & \sqrt{N_c - N_s - N_b + 1} \\ \sqrt{(N_c - N_s - N_b + 1)(N_b - 1)} & N_c + N_b - 1 & \sqrt{(N_s - 1)(N_b - 1)} & \sqrt{N_b - 1} \\ \sqrt{(N_c - N_s - N_b + 1)(N_s - 1)} & \sqrt{(N_s - 1)(N_b - 1)} & N_c + N_s - 1 & \sqrt{N_s - 1} \\ \sqrt{N_c - N_s - N_b + 1} & \sqrt{N_b - 1} & \sqrt{N_s - 1} & 2N_c + 1 \end{pmatrix}. \tag{C2}$$

If we just keep the leading terms in the limit of $1 \ll N_s, N_s \ll N_c$, it becomes

$$H \approx -|y_s, y_b\rangle\langle y_s, y_b| - 2|g_s, g_b\rangle\langle g_s, g_b|$$
$$- |y_s, g_b\rangle\langle y_s, g_b| - |g_s, y_b\rangle\langle g_s, y_b|$$
$$- \sqrt{\frac{N_s}{N_c}}(|y_s, y_b\rangle\langle y_s, g_b| + |y_s, g_b\rangle\langle y_s, y_b|)$$
$$- \sqrt{\frac{N_b}{N_c}}(|y_s, y_b\rangle\langle g_s, y_b| + |g_s, y_b\rangle\langle y_s, y_b|). \tag{C3}$$

Its eigenenergies are

$$E_0 = -2, \tag{C4}$$

$$E_1 = -1 - \sqrt{\frac{N_s + N_b}{N_c}}, \tag{C5}$$

$$E_2 = -1, \tag{C6}$$

$$E_3 = -1 + \sqrt{\frac{N_s + N_b}{N_c}}. \tag{C7}$$

The corresponding eigenstates are

$$|\Psi_0\rangle = \begin{pmatrix} 0 \\ 0 \\ 0 \\ 1 \end{pmatrix}, \quad |\Psi_1\rangle = \begin{pmatrix} \frac{1}{\sqrt{2}} \\ \sqrt{\frac{N_s}{2(N_s+N_b)}} \\ \sqrt{\frac{N_b}{2(N_s+N_b)}} \\ 0 \end{pmatrix}, \tag{C8}$$

$$|\Psi_2\rangle = \begin{pmatrix} 0 \\ -\sqrt{\frac{N_b}{N_s+N_b}} \\ \sqrt{\frac{N_s}{N_s+N_b}} \\ 0 \end{pmatrix}, \quad |\Psi_3\rangle = \begin{pmatrix} -\frac{1}{\sqrt{2}} \\ \sqrt{\frac{N_s}{2(N_s+N_b)}} \\ \sqrt{\frac{N_b}{2(N_s+N_b)}} \\ 0 \end{pmatrix}. \tag{C9}$$

The time-dependent wave function with initial condition $|\Psi_{in}\rangle = \sqrt{1/N_s}|g_s, g_b\rangle + \sqrt{(N_s-1)/N_s}|y_s, g_b\rangle$ is

$$|\Psi\rangle = e^{-iE_0 t}\sqrt{\frac{1}{N_s}}|\Psi_0\rangle + \sqrt{\frac{N_s - 1}{N_s}}$$
$$\times \frac{\sqrt{\frac{N_s}{2}}(e^{-iE_3 t}|\Psi_3\rangle + e^{-iE_1 t}|\Psi_1\rangle) - e^{-iE_2 t}\sqrt{N_b}|\Psi_2\rangle}{\sqrt{N_s + N_b}}. \tag{C10}$$

Expanding it, we obtain Eq. (9) in the main text.

APPENDIX D: EXCLUSIVE-OR

The module 2 addition "$\oplus$" is also called the exclusive-OR (XOR) operation for two Boolean variables, which is defined as $0 \oplus 0 = 1 \oplus 1 = 0$ and $0 \oplus 1 = 1 \oplus 0 = 1$. For an integer i, the relation with its binary digits $i^{(m)}$ is

$$i = \sum_{m=0}^{n-1} 2^m i^{(m)}. \tag{D1}$$

For any two integers i_s and j_b, $v = i_s \oplus j_b$ is defined bitwise as (see Fig. 5)

$$v^{(m)} = i_s^{(m)} \oplus j_b^{(m)}. \tag{D2}$$

It can also be written as

$$v = i_s \oplus j_b = \sum_{m=0}^{n-1} 2^m\left(i_s^{(m)} \oplus j_b^{(m)}\right). \tag{D3}$$

For example, $12 \oplus 10 = 1100 \oplus 1010 = 0110 = 6$. There is an inverse relation that $j_b = i_s \oplus v$ if $v = i_s \oplus j_b$. We can check that $12 \oplus 6 = 1100 \oplus 0110 = 1010 = 10$.
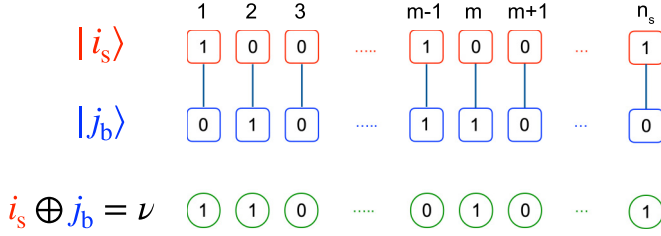
FIG. 5. Illustration of $i_s \oplus j_b = \nu$. Red squares represent qubits of the system; blue squares represent qubits of the bath; the vertical lines represent the pairwise interaction $\hat{s}_m^x \hat{\sigma}_m^x$ between the system qubits and bath qubits. The binary digits of ν are placed in circles for clarity.

APPENDIX E: ANALYSIS OF THE LOCAL HAMILTONIAN

The Hamiltonian with local interaction is [Eqs. (6) and (13) in the main text]

$$H = -|g_s\rangle\langle g_s| - |g_b\rangle\langle g_b| - \lambda_{n_s} \sum_{m=0}^{n_s-1} \hat{s}_m^x \hat{\sigma}_m^x. \quad (E1)$$

The decomposition of its Hilbert space is possible due to the parity between system qubits and bath qubits. For a pair of states $|i_s\rangle$ and $|j_b\rangle$, this parity is given by a number $\nu = i_s \oplus j_b$, where $\oplus$ is a bitwise module 2 addition as illustrated in Fig. 5. Since $[\hat{s}_m^z \hat{\sigma}_m^z, H] = 0$, the parity number ν is conserved during the dynamical evolution.

We define a sub-Hilbert space $\mathcal{H}_\nu$, which is spanned by all $|i_s, j_b\rangle$'s satisfying $i_s \oplus j_b = \nu$. Because of $j_b = i_s \oplus \nu$, there is one-to-one mapping between the system states $|i_s\rangle$ and the bath states $|j_b\rangle$ in each subspace $\mathcal{H}_\nu$. Therefore, each Hilbert space $\mathcal{H}_\nu$ is of dimension N_s. The subspace $\mathcal{H}_\nu$ is invariant under the unitary transformation of the total Hamiltonian H. As a result, the whole dynamical evolution is just a simple summation of dynamics in each subspace $\mathcal{H}_\nu$.

Therefore, we can independently investigate the dynamical evolution within each subspace. In a given subspace $\mathcal{H}_{\nu_{j_s}}$ (j_s is one of i_s's), there are only two on-site energy terms in Eq. (E1), and the total Hamiltonian is reduced to

$$H_{j_s} = -|g_s, j_b\rangle\langle g_s, j_b| - |j_s, g_b\rangle\langle j_s, g_b| - \lambda_{n_s}\sum_{m=0}^{n_s-1}\hat{s}_m^x \hat{\sigma}_m^x. \quad (E2)$$

In the subspace $\mathcal{H}_{\nu_{j_s}}$, there is one-to-one mapping between $|i_s\rangle$ and $|j_b\rangle$ via $i_s \oplus j_b = \nu_{j_s}$. As a result, we can hide the bath qubits and simplify the above Hamiltonian in the subspace as

$$H_{j_s} = -|g_s\rangle\langle g_s| - |j_s\rangle\langle j_s| - \lambda_{n_s}\sum_{m=0}^{n_s-1}\hat{s}_m^x, \quad (E3)$$

which is Eq. (14) in the main text.

The numerical results of evolution with Hamiltonian Eq. (E1) are calculated. The probability of the ground state of the problem system is shown in Fig. 6. Figure 6(a) displays the oscillations of the ground-state probability with $l_j = \lfloor n_s/2 \rfloor$, and Fig. 6(b) shows the oscillations with $l_j = n_s$. Their oscillation involves sinelike functions in different subspaces. The period of (b) is larger than (a) because of the longer Ham-
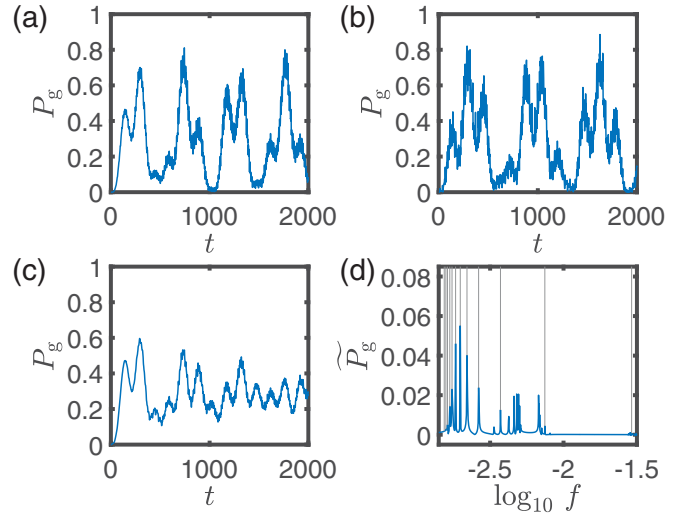

FIG. 6. The evolution with the Hamiltonian in Eq. (E1) with $n_s = n_b = 12$. The interaction strength is $\gamma_1 = 1$, $\gamma_2 = 1.16$, and $\gamma_{m\geqslant 3} = 0$. P_g is the time dependent ground-state probability of the problem system. For (a) and (b), the initial condition is $|\Psi_{\text{in}}\rangle = |j_s, g_b\rangle$ with Hamming distance (a) $l_j = 6$ and (b) $l_j = 12$. (c) The initial state is $|\Psi_{\text{in}}\rangle = \sqrt{1/N_s}\sum_{j_s=0}^{N_s-1}|j_s, g_b\rangle$. (d) The Fourier transformation of (c). The gray line shows the peaks contributed by different l_j.

ming distance. The oscillations with $l_j = n_s$ have the largest timescale, which corresponds to the full thermal equilibrium. The evolution with the initial state Eq. (8) in the main text is shown in Fig. 6(c), where the increasing slope near $t = 0$ is seen to be similar to (a). This indicates that the problem system can be cooled down considerably earlier than the equilibrium between the bath and the problem system is reached. Figure 6(d) is the Fourier transformation of (c). Peaks for independent oscillations with different l_j are clearly visible.

The wave packet $|\chi_g\rangle$ located near $|g_s\rangle$ of Eq. (14) can be approximated analytically. We rearrange the basis and write $|\chi_g\rangle$ as

$$|\chi_g\rangle = \sum_{h=0}^{n_s}\sum_{m=1}^{C_{n_s}^h} a_{h,m}|\psi_{h,m}\rangle, \quad (E4)$$

where $|\psi_{h,m}\rangle$'s are rearranged $|i_s\rangle$'s with Hamming distance h from $|g_s\rangle$, so that $|\psi_{h=0}\rangle = |g_s\rangle$. m labels the different states with the same h. The 2^{n_s} vertices of the hypercube can be viewed as points on the surface of an n_s-dimensional hypersphere, as seen in Fig. 3(b) in the main text. There are $C_{n_s}^h$ points located on the same latitude of the hypersphere, which have the same h. When $|\chi_j\rangle$ is far from $|\chi_g\rangle$ with $l_j \gg 1$, the influence of $|\chi_j\rangle$ is so small that $|\chi_g\rangle$ has rotation symmetry with the coefficients independent of m, i.e.,

$$a_{h,m} \approx a_h. \quad (E5)$$

Numerically computed $a_{h,m}$ are shown in Fig. 3(c) in the main text, where each blue point represents one $a_{h,m}$. It is clear from the figure that the $C_{n_s}^h$ points with the same h are nearly identical. They become visibly different only near the location of $|j_s\rangle$, i.e., at $h = 9$ in this example. Most $a_{h,m}$ have the same sign except some near $|j_s\rangle$. The interaction $\sum_{m=0}^{n_s-1}\hat{s}_m^x$ only changes one qubit, so each point at the hth will interact

with h points at the $(h-1)$th and $n_s - h$ points at $(h+1)$th as shown by the yellow line in Fig. 3(b). If we neglect the term $-|j_s\rangle\langle j_s|$ using a tight-binding approximation, the eigenequation for Eq. (14) can be written as

$$-h\lambda_{n_s}a_{h-1} + Va_h - (n_s - h)\lambda_{n_s}a_{h+1} = Ea_h, \quad \text{(E6)}$$

where $V = -1$ if $h = 0$ and $V = 0$ if $h \geqslant 1$.

a_h could be approached analytically using the iteration method. We rewrite Eq. (E6) as

$$-h\lambda_{n_s}a_{h-1} + Va_h - (n_s - h)\lambda_{n_s}a_{h+1} = Ea_h, \quad \text{(E7)}$$

where $V = -1$ if $h = 0$ and $V = 0$ if $h \geqslant 1$. We rewrite it as

$$(-1 - E)a_0 - n_s\lambda a_1 = 0,$$
$$-h\lambda a_{h-1} - Ea_h - (n_s - h)\lambda a_{h+1} = 0 \ (1 \leqslant h \leqslant n_s). \quad \text{(E8)}$$

We define the ratio $b_h = a_h/a_{h-1}$ and get

$$b_h = \frac{h\lambda}{1 + n_s\lambda b_1 - (n_s - h)\lambda b_{n+1}}. \quad \text{(E9)}$$

With the self-consistent method, the above iteration becomes

$$b_h^{(m+1)} = \frac{h\lambda}{1 + n_s\lambda b_1^{(m)} - (n_s - h)\lambda b_{h+1}^{(m)}}, \quad \text{(E10)}$$

where the superscript is the order of approximation. If we set $b_h^{(0)} = 0$, we get

$$b_h^{(1)} = h\lambda, \quad \text{(E11)}$$

$$b_h^{(2)} = \frac{h\lambda}{1 + n_s\lambda^2 - (n_s - h)(h+1)\lambda^2}, \quad \text{(E12)}$$

$$b_h^{(3)} = \frac{h\lambda}{1 + \frac{n_s\lambda^2}{1-(n_s-2)\lambda^2} - \frac{(n_s-h)(h+1)\lambda^2}{1+n_s\lambda^2-(n_s-h-1)(h+2)\lambda^2}}. \quad \text{(E13)}$$

The corresponding energy is

$$E^{(1)} = -1 - n_s\lambda^2, \quad \text{(E14)}$$

$$E^{(2)} = -1 - \frac{n_s\lambda^2}{1 - (n_s - 2)\lambda^2}, \quad \text{(E15)}$$

$$E^{(3)} = -1 - \frac{n_s\lambda^2}{1 + \frac{n_s\lambda^2}{1-(n_s-2)\lambda^2} - \frac{2(n_s-1)\lambda^2}{1-(2n_s-6)\lambda^2}}. \quad \text{(E16)}$$

We define $a_0 = 1/\sqrt{\aleph}$, where $\aleph$ is the normalization factor. The coefficient for $h \geqslant 1$ is

$$a_h = \frac{1}{\sqrt{\aleph}}\prod_{m=1}^{h} b_m. \quad \text{(E17)}$$

The first-order approximation is

$$a_h^{(1)} = \frac{1}{\sqrt{\aleph^{(1)}}}\frac{h!}{n_s^h}\lambda^h \approx \sqrt{\frac{2\pi h}{\aleph^{(1)}}}\left(\frac{h}{en_s}\right)^h, \quad \text{(E18)}$$

where the last term is obtained with the Stirling approximation. It is accurate only in the regime $h \geqslant 1$ and $h/n_s < 0.2$. By fitting the numerical data in Fig. 3(c) in the main text, we find that the decay speed of a_h is exponential in the regime $h/n_s < 0.2$ and inversely proportional to h in the regime $h/n_s > 0.3$.
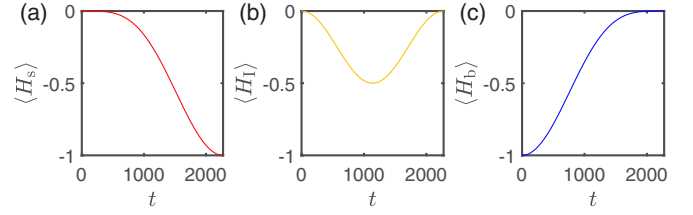

FIG. 7. The time-dependent energy variation according to Eq. (C2). The parameters are $N_s = N_b = 2^{20}$. (a) The energy of the problem system. (b) The coupling energy between the problem system and the bath. (c) The energy of the bath.

APPENDIX F: COMPARISON TO CONVENTIONAL COOLING

In conventional cooling, the interaction between the system and the bath is limited to the interface. As a result, the interaction energy $\langle H_I\rangle$ is much smaller than both the system energy $\langle H_s\rangle$ and the bath energy $\langle H_b\rangle$. During the cooling process, the total energy $\langle H_s + H_b\rangle$ can be approximately regarded as conserved. In addition, the cooling process is usually complicated. The quantum dynamics for the composite system, the system plus the bath, is ergodic and irreversible.

Cooling has been developed in practice and generalized in conception. The constraints discussed above are not essential. For example, in laser cooling, as each atom in the gas interacts with the photons from the laser, the interaction energy $\langle H_I\rangle$ is comparable to the system energy $\langle H_s\rangle$ [61,62]. Evaporative cooling of atomic gases is more aggressive, and over 90% of the system is removed after the cooling [62].

The quantum adiabatic algorithm (QAA) is also called quantum annealing, a cooling process. During the annealing, the bath only appears as a parameter in the Hamiltonian. After QAA was proposed, it was immediately compared to conventional cooling. Its quantum advantage was only confirmed after the quantum adiabatic search algorithm was proposed and shown to be as fast as Grover's algorithm.

The quantum icebox algorithm proposed in this work is a conceptual generalization of conventional cooling. In this kind of quantum icebox cooling, the interaction energy $\langle H_I\rangle$ is usually comparable to the system energy $\langle H_s\rangle$. To demonstrate its quantum advantage, we have applied it to an idealized system, similar to the one used in the quantum adiabatic search algorithm. In particular, for the nonlocal interaction, the cooling dynamics becomes periodic and nonergodic. However, even in this case, as seen in Fig. 7, for the first half of the oscillation, the system energy decreases with time while the bath energy increases with time, a typical feature of cooling.

APPENDIX G: HIGH-ORDER TRANSITION

For the composite system $H_0 = H_s + H_b$, the cooling starts when the interaction H_I is turned on, making the transition between different eigenstates $|i_s, \phi_{j_b}\rangle$ of H_0 possible. The transition probability can be written as [63]

$$W_{i_s', \phi_{j_b'}, i_s, \phi_{j_b}} = \frac{2\pi}{\hbar}|\langle i_s', \phi_{j_b'}|T^+(E_{i_s, j_b})|i_s, \phi_{j_b}\rangle|\delta$$
$$\times (E_{i_s', \phi_{j_b'}} - E_{i_s, \phi_{j_b}}), \quad \text{(G1)}$$

where

$$T^+(E) = H_I + H_I G_0^+(E) H_I + H_I G_0^+(E) H_I G_0^+(E) H_I + \cdots$$
(G2)

with $G_0^+(E) = \lim_{\epsilon \to 0^+} (E + i\epsilon - H_0)^{-1}$ being the noninteracted Green's function in the upper plane. Fermi's "golden rule" is obtained at the cutoff of $T^+(E) \approx H_I$. In the finite time case, the δ function will broaden to a smooth function.

When H_I is k-local, which is true for many realistic physical systems, each application of operator H_I changes at most $k-1$ qubits in the problem system. The mth-order term in Eq. (G2) represents a transition where H_I is applied m times. In the first-order approximation, only the states with Hamming distance less than k from the ground state $|g_s\rangle$ have nonzero transition probability, which spans a space of much lower dimension than the whole Hilbert space N_s. For the unstructured search problem, the initial state of the problem system is an equal superposition of all the states. For the first-order transition, only $O(n_s^{k-1})$ components among the N_s terms in the initial state can be cooled down, the successful probability of which is $O(n_s^{k-1}/N_s)$. The interaction strength is normalized to $O(1/n_s^{k-1})$. The average cooling time is inversely proportional to the product of the interaction strength and successful probability, which is $O(N_s)$. This shows that the cooling speed will be reduced to the classical speed if just the first-order term is considered.

A similar low-order cooling process happens with a Markovian bath [39–43]. In the Markovian master equation, only low orders of transition are taken into consideration. The bath is only allowed to absorb local energy using low orders of a k-local interaction. This makes it difficult for a Markovian bath to cool down the system efficiently. In particular, processes in which the system we want to cool first increases in energy do not come into play with a zero-temperature Markovian bath.

In contrast, the coherent bath with non-Markovian dynamics allows more general cooling paths. When $\langle H_I \rangle$ is comparable to $\langle H_s \rangle$, the convergence of Eq. (G2) becomes slow. All these small transitions act together to flip about $n_s/2$ qubits coherently, reducing the cooling time to $O(\sqrt{N_s})$. It is essentially a tunneling effect, where the quantum state effectively arrives at the "forbidden" side of a high, wide energy barrier.

APPENDIX H: COMPARISON TO OTHER ALGORITHMS

It is appropriate to compare our work with the more familiar QAA or quantum annealing. Although it is based on significantly different principles, the Hamiltonians of the computational qubit and the initial-state preparation used in our quantum icebox algorithm are widely used in QAA [21,64–67]. Thus, the experimental systems used to implement QAA [65,68] and quantum simulation [69,70] can be modified to explore our icebox strategy. The icebox strategy might have practical advantages. During the process of continuously changing the Hamiltonian in QAA, the system is vulnerable to external heat or noise [71–73], because it often encounters an exponentially small energy gap [74]. The low-temperature bath is more forgiving.

Our quantum icebox algorithm also differs from the heat-bath algorithmic cooling (HBAC) and interaction-enhanced quantum computing, both in design and scope. HBAC is used to purify a known ground state [48–52], while interaction-enhanced quantum computing exploits different quantum computers [53], as opposed to a computer and a bath.

[1] L. K. Grover, A fast quantum mechanical algorithm for database search, in *Proceedings of the Twenty-Eighth Annual ACM Symposium on Theory of Computing*, STOC '96 (ACM Press, New York, 1996), pp. 212–219.

[2] P. W. Shor, Polynomial-time algorithms for prime factorization and discrete logarithms on a quantum computer, SIAM Rev. **41**, 303 (1999).

[3] N. W. Hendrickx, D. P. Franke, A. Sammak, G. Scappucci, and M. Veldhorst, Fast two-qubit logic with holes in germanium, Nature (London) **577**, 487 (2020).

[4] L. Petit, H. G. J. Eenink, M. Russ, W. I. L. Lawrie, N. W. Hendrickx, S. G. J. Philips, J. S. Clarke, L. M. K. Vandersypen, and M. Veldhorst, Universal quantum logic in hot silicon qubits, Nature (London) **580**, 355 (2020).

[5] E. Farhi and S. Gutmann, Analog analogue of a digital quantum computation, Phys. Rev. A **57**, 2403 (1998).

[6] E. Farhi, J. Goldstone, S. Gutmann, and M. Sipser, Quantum computation by adiabatic evolution, arXiv:quant-ph/0001106.

[7] D. Aharonov, W. van Dam, J. Kempe, Z. Landau, S. Lloyd, and O. Regev, Adiabatic quantum computation is equivalent to standard quantum computation, SIAM J. Comput. **37**, 166 (2007).

[8] H. Yu, Y. Huang, and B. Wu, Exact equivalence between quantum adiabatic algorithm and quantum circuit algorithm, Chin. Phys. Lett. **35**, 110303 (2018).

[9] W. van Dam, M. Mosca, and U. Vazirani, How powerful is adiabatic quantum computation?, in *Proceedings of the 42nd IEEE Symposium on Foundations of Computer Science* (IEEE, Piscataway, NJ, 2001), pp. 279–287.

[10] I. Ozfidan, C. Deng, A.Y. Smirnov, T. Lanting, R. Harris, L. Swenson, J. Whittaker, F. Altomare, M. Babcock, C. Baron, A.J. Berkley, K. Boothby, H. Christiani, P. Bunyk, C. Enderud, B. Evert, M. Hager, A. Hajda, J. Hilton, S. Huang *et al.*, Demonstration of a Nonstoquastic Hamiltonian in Coupled Superconducting Flux Qubits, Phys. Rev. Applied **13**, 034037 (2020).

[11] F. Wilczek, H.-Y. Hu, and B. Wu, Resonant quantum search with monitor qubits, Chin. Phys. Lett. **37**, 050304 (2020).

[12] E. Farhi and S. Gutmann, Quantum computation and decision trees, Phys. Rev. A **58**, 915 (1998).

[13] S. O. Valenzuela, W. D. Oliver, D. M. Berns, K. K. Berggren, L. S. Levitov, and T. P. Orlando, Microwave-induced cooling of a superconducting qubit, Science **314**, 1589 (2006).

[14] X. Xu, Y. Wu, B. Sun, Q. Huang, J. Cheng, D. G. Steel, A. S. Bracker, D. Gammon, C. Emary, and L. J. Sham, Fast Spin State Initialization in a Singly Charged InAs-GaAs Quantum Dot by Optical Cooling, Phys. Rev. Lett. **99**, 097401 (2007).

[15] D. Press, T. D. Ladd, B. Zhang, and Y. Yamamoto, Complete quantum control of a single quantum dot spin using ultrafast optical pulses, Nature (London) **456**, 218 (2008).

[16] E. Togan, Y. Chu, A. Imamoglu, and M. D. Lukin, Laser cooling and real-time measurement of the nuclear spin environment of a solid-state qubit, Nature (London) **478**, 497 (2011).

[17] B. Yang, H. Sun, C.-J. Huang, H.-Y. Wang, Y. Deng, H.-N. Dai, Z.-S. Yuan, and J.-W. Pan, Cooling and entangling ultracold atoms in optical lattices, Science **369**, 550 (2020).

[18] L. K. Grover, Quantum Mechanics Helps in Searching for a Needle in a Haystack, Phys. Rev. Lett. **79**, 325 (1997).

[19] L. K. Grover, Quantum Computers Can Search Rapidly by Using Almost Any Transformation, Phys. Rev. Lett. **80**, 4329 (1998).

[20] M. A. Nielsen and I. L. Chuang, *Quantum Computation and Quantum Information: 10th Anniversary Edition* (Cambridge University Press, Cambridge, 2010).

[21] A. Lucas, Ising formulations of many np problems, Front. Phys. **2**, 5 (2014).

[22] F. Franchini, *An Introduction to Integrable Techniques for One-Dimensional Quantum Systems* (Springer, Cham, 2017).

[23] N. Gromov, F. Levkovich-Maslyuk, and G. Sizov, New construction of eigenstates and separation of variables for SU(N) quantum spin chains, J. High Energy Phys. 09, 111 (2017).

[24] O. Salberger and V. Korepin, Entangled spin chain, Rev. Math. Phys. **29**, 1750031 (2017).

[25] P. N. Jepsen, J. Amato-Grill, I. Dimitrova, W. W. Ho, E. Demler, and W. Ketterle, Spin transport in a tunable heisenberg model realized with ultracold atoms, Nature (London) **588**, 403 (2020).

[26] B. Bertini, M. Collura, J. De Nardis, and M. Fagotti, Transport in Out-Of-Equilibrium *xxz* Chains: Exact Profiles of Charges and Currents, Phys. Rev. Lett. **117**, 207201 (2016).

[27] O. A. Castro-Alvaredo, B. Doyon, and T. Yoshimura, Emergent Hydrodynamics in Integrable Quantum Systems Out of Equilibrium, Phys. Rev. X **6**, 041065 (2016).

[28] Y. Hu, Z. Zhang, and B. Wu, Quantum algorithm for a set of quantum 2sat problems, Chin. Phys. B **30**, 020308 (2021).

[29] K. Vandaele, S. J. Watzman, B. Flebus, A. Prakash, Y. Zheng, S. R. Boona, and J. P. Heremans, Thermal spin transport and energy conversion, Mater. Today Phys. **1**, 39 (2017).

[30] C. Liu, J. Chen, T. Liu, F. Heimbach, H. Yu, Y. Xiao, J. Hu, M. Liu, H. Chang, T. Stueckler, S. Tu, Y. Zhang, Y. Zhang, P. Gao, Z. Liao, D. Yu, K. Xia, N. Lei, W. Zhao, and M. Wu, Long-distance propagation of short-wavelength spin waves, Nat. Commun. **9**, 738 (2018).

[31] M. Boyer, G. Brassard, P. Høyer, and A. Tapp, Tight bounds on quantum searching, Fortschr. Phys. **46**, 493 (1998).

[32] P. R. Giri and V. E. Korepin, A review on quantum search algorithms, Quantum Inf. Process. **16**, 315 (2017).

[33] J. Roland and N. J. Cerf, Quantum search by local adiabatic evolution, Phys. Rev. A **65**, 042308 (2002).

[34] X. Wang, A. Sørensen, and K. Mølmer, Multibit Gates for Quantum Computing, Phys. Rev. Lett. **86**, 3907 (2001).

[35] E. Farhi, J. Goldstone, and S. Gutmann, Quantum adiabatic evolution algorithms versus simulated annealing, arXiv:quant-ph/0201031.

[36] X. He, S. Chen, and G. D. Doolen, A novel thermal model for the lattice boltzmann method in incompressible limit, J. Comput. Phys. **146**, 282 (1998).

[37] J. S. Wang, J. Wang, and J. T. Lü, Quantum thermal transport in nanostructures, Eur. Phys. J. B **62**, 381 (2008).

[38] K. Sääskilahti, J. Oksanen, and J. Tulkki, Thermal balance and quantum heat transport in nanostructures thermalized by local langevin heat baths, Phys. Rev. E **88**, 012128 (2013).

[39] M. Silveri, H. Grabert, S. Masuda, K. Y. Tan, and M. Möttönen, Theory of quantum-circuit refrigeration by photon-assisted electron tunneling, Phys. Rev. B **96**, 094524 (2017).

[40] H. Hsu, M. Silveri, A. Gunyhó, J. Goetz, G. Catelani, and M. Möttönen, Tunable refrigerator for nonlinear quantum electric circuits, Phys. Rev. B **101**, 235422 (2020).

[41] B. M. Terhal and D. P. DiVincenzo, Problem of equilibration and the computation of correlation functions on a quantum computer, Phys. Rev. A **61**, 022301 (2000).

[42] M. Metcalf, J. E. Moussa, W. A. de Jong, and M. Sarovar, Engineered thermalization and cooling of quantum many-body systems, Phys. Rev. Research **2**, 023214 (2020).

[43] K. Y. Tan, M. Partanen, R. E. Lake, J. Govenius, S. Masuda, and M. Möttönen, Quantum-circuit refrigerator, Nat. Commun. **8**, 15189 (2017).

[44] M. Raghunandan, F. Wolf, C. Ospelkaus, P. O. Schmidt, and H. Weimer, Initialization of quantum simulators by sympathetic cooling, Sci. Adv. **6**, eaaw9268 (2020).

[45] S. Polla, Y. Herasymenko, and T. E. O'Brien, Quantum digital cooling, Phys. Rev. A **104**, 012414 (2021).

[46] O. F. Syljuåsen and A. W. Sandvik, Quantum Monte Carlo with directed loops, Phys. Rev. E **66**, 046701 (2002).

[47] T. J. Yoder, G. H. Low, and I. L. Chuang, Fixed-Point Quantum Search with an Optimal Number of Queries, Phys. Rev. Lett. **113**, 210501 (2014).

[48] P. O. Boykin, T. Mor, V. Roychowdhury, F. Vatan, and R. Vrijen, Algorithmic cooling and scalable NMR quantum computers, Proc. Natl. Acad. Sci. USA **99**, 3388 (2002).

[49] N. A. Rodríguez-Briones and R. Laflamme, Achievable Polarization for Heat-Bath Algorithmic Cooling, Phys. Rev. Lett. **116**, 170501 (2016).

[50] S. Raeisi, M. Kieferová, and M. Mosca, Novel Technique for Robust Optimal Algorithmic Cooling, Phys. Rev. Lett. **122**, 220501 (2019).

[51] S. Raeisi and M. Mosca, Asymptotic Bound for Heat-Bath Algorithmic Cooling, Phys. Rev. Lett. **114**, 100404 (2015).

[52] S. Zaiser, C. T. Cheung, S. Yang, D. B. R. Dasari, S. Raeisi, and J. Wrachtrup, Cyclic cooling of quantum systems at the saturation limit, npj Quantum Inf. **7**, 92 (2021).

[53] A. Shi, H. Guan, J. Zhang, and W. Zhang, Long-range interaction enhanced adiabatic quantum computers, Chin. Phys. Lett. **37**, 120301 (2020).

[54] P. A. Camati, J. F. G. Santos, and R. M. Serra, Employing non-Markovian effects to improve the performance of a quantum otto refrigerator, Phys. Rev. A **102**, 012217 (2020).

[55] J. M. Zhang and Y. Liu, Fermi's golden rule: Its derivation and breakdown by an ideal model, Eur. J. Phys. **37**, 065406 (2016).

[56] C. Mochon, Hamiltonian oracles, Phys. Rev. A **75**, 042313 (2007).

[57] Y. Tanaka, T. Ichikawa, M. Tada-Umezaki, Y. Ota, and M. Nakahara, Quantum oracles in terms of universal gate set, Int. J. Quantum Inf. **09**, 1363 (2011).

[58] H. Ito and S. Iida, Method for organizing grover's quantum oracle, Open Syst. Inf. Dyn. **21**, 1450011 (2014).

[59] O. Katz, M. Cetina, and C. Monroe, *n*-body interactions between trapped ion qubits via spin-dependent squeezing, arXiv:2202.04230.

[60] M. Saffman, T. G. Walker, and K. Mølmer, Quantum information with rydberg atoms, Rev. Mod. Phys. **82**, 2313 (2010).

[61] D. Leibfried, R. Blatt, C. Monroe, and D. Wineland, Quantum dynamics of single trapped ions, Rev. Mod. Phys. **75**, 281 (2003).

[62] V. I. Yukalov, Basics of Bose-Einstein condensation, Phys. Part. Nuclei **42**, 460 (2011).

[63] E. N. Economou, *Green's Functions in Quantum Physics* (Springer, Berlin, Heidelberg, 2006).

[64] E. Farhi, J. Goldstone, S. Gutmann, J. Lapan, A. Lundgren, and D. Preda, A quantum adiabatic evolution algorithm applied to random instances of an np-complete problem, Science **292**, 472 (2001).

[65] M. W. Johnson, M. H. S. Amin, S. Gildert, T. Lanting, F. Hamze, N. Dickson, R. Harris, A. J. Berkley, J. Johansson, P. Bunyk, E. M. Chapple, C. Enderud, J. P. Hilton, K. Karimi, E. Ladizinsky, N. Ladizinsky, T. Oh, I. Perminov, C. Rich, M. C. Thom *et al.*, Quantum annealing with manufactured spins, Nature (London) **473**, 194 (2011).

[66] C. C. McGeoch, Adiabatic quantum computation and quantum annealing: Theory and practice, Synthesis Lect. Quantum Comput. **5**, 1 (2014).

[67] X. Qiu, P. Zoller, and X. Li, Programmable quantum annealing architectures with ising quantum wires, PRX Quantum **1**, 020311 (2020).

[68] R. Harris, J. Johansson, A. J. Berkley, M. W. Johnson, T. Lanting, S. Han, P. Bunyk, E. Ladizinsky, T. Oh, I. Perminov, E. Tolkacheva, S. Uchaikin, E. M. Chapple, C. Enderud, C. Rich, M. Thom, J. Wang, B. Wilson, and G. Rose, Experimental demonstration of a robust and scalable flux qubit, Phys. Rev. B **81**, 134510 (2010).

[69] C. Monroe, W. C. Campbell, L.-M. Duan, Z.-X. Gong, A. V. Gorshkov, P. W. Hess, R. Islam, K. Kim, N. M. Linke, G. Pagano, P. Richerme, C. Senko, and N. Y. Yao, Programmable quantum simulations of spin systems with trapped ions, Rev. Mod. Phys. **93**, 025001 (2021).

[70] S. Ebadi, T. T. Wang, H. Levine, A. Keesling, G. Semeghini, A. Omran, D. Bluvstein, R. Samajdar, H. Pichler, W. W. Ho, S. Choi, S. Sachdev, M. Greiner, V. Vuletić, and M. D. Lukin, Quantum phases of matter on a 256-atom programmable quantum simulator, Nature (London) **595**, 227 (2021).

[71] E. Paladino, Y. M. Galperin, G. Falci, and B. L. Altshuler, 1/f noise: Implications for solid-state quantum information, Rev. Mod. Phys. **86**, 361 (2014).

[72] A. Bilmes, S. Zanker, A. Heimes, M. Marthaler, G. Schön, G. Weiss, A. V. Ustinov, and J. Lisenfeld, Electronic decoherence of two-level systems in a josephson junction, Phys. Rev. B **96**, 064504 (2017).

[73] J. Braumüller, L. Ding, A. P. Vepsäläinen, Y. Sung, M. Kjaergaard, T. Menke, R. Winik, D. Kim, B. M. Niedzielski, A. Melville, J. L. Yoder, C. F. Hirjibehedin, T. P. Orlando, S. Gustavsson, and W. D. Oliver, Characterizing and Optimizing Qubit Coherence Based on SQUID Geometry, Phys. Rev. Appl. **13**, 054079 (2020).

[74] A. P. Young, S. Knysh, and V. N. Smelyanskiy, Size Dependence of the Minimum Excitation Gap in the Quantum Adiabatic Algorithm, Phys. Rev. Lett. **101**, 170503 (2008).